ON THE NEAR-EARTH OBSERVATION OF PROTONS AND ELECTRONS FROM THE DECAY OF LOW-ENERGY SOLAR FLARE NEUTRONS

NEUS AGUEDA[1,2], SÄM KRUCKER[1,3], ROBERT P. LIN[1,4], AND LINGHUA WANG[1]
[1] Space Sciences Laboratory, University of California, Berkeley, CA, USA
[2] Departament d'Astronomia i Meteorologia, Institut de Ciències del Cosmos (ICC), Universitat de Barcelona, Spain
[3] Institute of 4D Technologies, School of Engineering, University of Applied Sciences Northwestern Switzerland, Windisch, Switzerland
[4] Physics Department, University of California, Berkeley, CA, USA

ABSTRACT

We investigate the near-Earth observation of interplanetary protons and electrons that result from the in-flight beta decay of low-energy (1–10 MeV) solar neutrons. We use in situ measurements throughout solar cycle 23 of 1–11 MeV protons and 50–400 keV electrons by the 3DP experiment on board the *Wind* spacecraft. We select a sample of isolated large (X-class) eastern hemisphere flares occurring during quiescent interplanetary conditions with the goal of discriminating neutron-decay particles from primary solar energetic particles. Unfortunately, all major flares of solar cycle 23 have to be excluded, with the largest flare in our sample being a X3.6 flare. For these relatively small event sizes, no in situ events due to the decay of solar flare neutrons are observed by *Wind*. From the one event with simultaneous γ-ray observations, we estimate the expected signal of neutron-decay protons in the *Wind*/3DP detectors. We use theoretical calculations of the spectrum of escaping neutrons at the Sun combined with an interplanetary propagation model to predict the neutron-decay proton spectrum expected near the Earth. We find that the expected spectrum is indeed well below the background intensities. However, using the estimates derived from the largest solar event of cycle 23 (2003 October 28) and assuming the flare would have occurred isolated in the eastern hemisphere, a clear signal above 5 MeV is expected to be seen.

Key words: Sun: flares – Sun: particle emission

Online-only material: color figures

1. INTRODUCTION

The observation of solar neutrons has long been recognized as a probe for learning about the properties of ions accelerated in solar flares (Lingenfelter & Ramaty 1967). Neutrons are produced in solar flares when accelerated ions interact in the chromosphere. There are a variety of interactions that produce neutrons, such as proton–proton, proton–α-particle, and α-particle–α-particle interactions (see, e.g., Ramaty & Murphy 1987; Hua et al. 2002). Alpha-particle interactions with nuclear species heavier than He dominate low-energy (1–10 MeV) neutron production for incident particle energies below about 30 MeV nucleon^{-1} (Share et al. 2011).

Detailed theoretical calculations of neutron production by flare-accelerated ion interactions (Hua & Lingenfelter 1987; Hua et al. 2002; Share et al. 2011) indicate that the spectrum of neutrons escaping the Sun is nearly flat at low energies (<10 MeV), with a steepening at higher energies. Therefore, a large fraction of neutrons is concentrated in the low-energy portion of the spectrum. Neutrons can be captured on ambient hydrogen in the photosphere, producing deuterium and a strong γ-ray line at 2.223 MeV.

Neutrons that escape from the Sun can be detected in space using in situ instruments. Previous studies have reported observations of solar neutrons at 1 AU by two methods: (1) the direct detection of solar neutrons by spacecraft detectors and ground level neutron monitors on Earth (e.g., Chupp et al. 1987; Shea et al. 1991; Ryan et al. 1993; Feldman et al. 2010) and (2) the measurement in space of particles which arise from the in-flight decay of energetic neutrons emitted at the Sun (Evenson et al. 1983; Ruffolo 1991; Dröge et al. 1996). These methods provide complementary information on the spectral, angular, and temporal distribution of solar neutrons, which can be used to constrain theoretical models of high-energy processes in solar flares.

To date, four energetic particle events produced by decaying solar flare neutrons have been observed (Evenson et al. 1983, 1985, 1990; Kocharov et al. 1996). These observations have proved to be a powerful tool to characterize the high-energy (>10 MeV) part of the neutron spectrum.

In Section 2 of this paper we review the interplanetary scenario for the observation of neutron-decay particles and we present a Monte Carlo simulation for the calculation of near-Earth neutron-decay proton intensities. In Section 3, we search throughout solar cycle 23 for neutron-decay particle events using in situ measurements of ≲10 MeV protons and 50–400 keV electrons by the Three-dimensional Plasma and Energetic Particle (3DP) experiment on board the *Wind* spacecraft (Lin et al. 1995). We select a sample of best-observed intense east hemisphere solar flares. Section 4 reviews the proton and electron measurements at 1 AU after each solar flare. We discuss the results in Section 5 and summarize this work in Section 6.

2. THEORY AND MODELING

2.1. Decay of Solar Neutrons in the Heliosphere

The decay of a free neutron follows the scheme $n \longrightarrow p + e^- + \bar{\nu}_e$, where n is a neutron, p is a proton, e^- is an electron, and $\bar{\nu}_e$ is an antineutrino. This process is energetically possible for a free neutron ($Q = 0.783$ MeV), which decays with a mean lifetime of $\tau_0 = 885$ s. Nearly the entire kinetic energy of the decaying neutron is transferred to the proton. The electron spectrum resulting from the decay of neutrons with a wide range of energies maintains an unchanging form for energies <1 MeV, with a peak around ~200 keV (Daibog & Stolpovskii 1987).
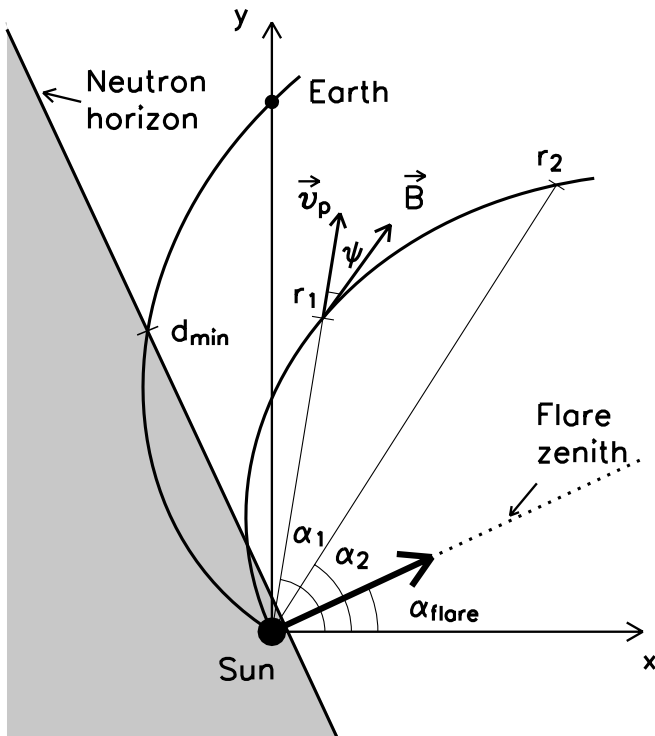
Figure 1. Solar system configuration in the ecliptic plane at the time of a solar flare. Neutrons from the flare have access only to the unshaded region of the figure. They propagate radially unaffected by the IMF until they decay. The daughter electrons and protons are trapped in the IMF. See the text for more details.

Given N_0 solar neutrons at $t = 0$, the number of neutrons N at some time t follows an exponential decay law given by

$$N = N_0 \exp\left(-t/\tau\right), \qquad (1)$$

where τ is the lifetime of a neutron moving at speed v, given by $\tau = \tau_0/\sqrt{1 - v^2/c^2}$, where τ_0 is the mean lifetime in the rest frame and c is the speed of light. Most ($\sim$63%) of the neutrons decay in the time interval $t \in [0, \tau]$, that is, at heliocentric distances $r < 0.1$ AU for 1 MeV neutrons; at $r < 0.3$ AU for 10 MeV and at $r < 0.5$ AU for 30 MeV neutrons.

The local solar horizon at the flare site, also known as neutron horizon, casts a shadow over one-half of the heliosphere (Evenson et al. 1983). Neutrons propagate into the non-obscured hemisphere along straight lines, unaffected by the interplanetary magnetic field (IMF). Solar neutrons only have access to the observer's field line outside the distance at which the neutron horizon intersects the observer's IMF line, $d_{\min}$ (see Figure 1). This minimal distance depends on the heliolongitude of the parent flare and the curvature of the IMF line, which in the Parker model of the IMF is determined by the solar wind speed (Parker 1958). From now on we will refer to this distance as the shadow radius.

Figure 2(a) shows $d_{\min}$ as a function of the solar flare location for different values of the solar wind speed. Figure 2(b) shows the percentage of remaining neutrons at $d_{\min}$ as a function of the location of the solar flare for three different neutron energies, 1 MeV, 10 MeV, and 30 MeV, assuming a solar wind speed of 400 km s^{-1}. It can be seen that for a given geometry of the solar system (solar wind speed and solar flare location), the smaller the solar wind speed, the larger the shadow radius. In addition, the smaller the neutron energy, the smaller the percentage of solar neutrons at the shadow radius. Low-energy
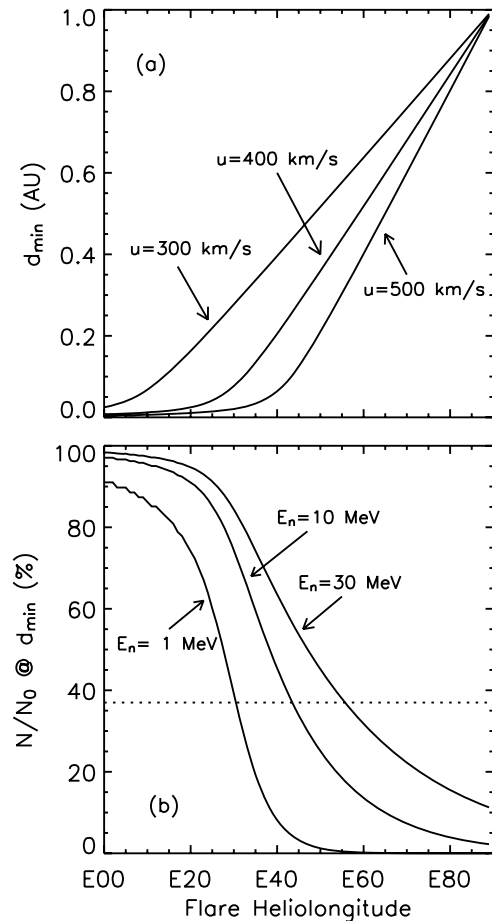

Figure 2. (a) Distance along the flare horizon to the observer's magnetic field line for different values of the solar wind speed and location of the solar flare; (b) percentage of remaining neutrons reaching $d_{\min}$ as a function of flare heliolongitude. We assume a solar wind speed of 400 km s^{-1}. The horizontal dotted line marks the 37% level.

($E < 10$ MeV) neutrons will usually be unobservable for flares at heliolongitudes greater than E45° (E60° for a solar wind speed of 600 km s^{-1}), for which the percentage of solar neutrons reaching the shadow radius is less than 37%.

The electrons and protons resulting from the decay of solar neutrons are trapped in the IMF, and they can be detected at any point in space magnetically connected to the location where the parent neutrons decayed. Therefore, it is in principle possible at 1 AU to observe particles from the in-flight decay of low-energy neutrons emitted from the Sun. However, the observation requires high neutron intensities, parent flare heliolongitudes smaller than E60°, stable IMF conditions, and periods of low solar energetic particle (SEP) intensities in the flux tube of the spacecraft.

Moreover, for a clear detection of neutron-decay particles, it is necessary to discriminate them from primary SEPs (Roelof 1966). This is possible for east hemisphere solar flares. Since solar neutrons propagate radially until they decay, instead of traveling diffusively along the Parker spiral (Parker 1958), the neutron-decay protons will show a precursor to the main in situ proton event.[5]

---

[5] Note that the observation of a precursor to the primary solar energetic particle event can be difficult for electrons, since primary flare electrons propagating scatter-free along the IMF can reach the observer before the bulk of neutron-decay electrons.

The first observation of energetic protons in interplanetary space attributed to the decay products of solar flare neutrons was observed on 1982 June 3, associated with an X8 γ-ray solar flare located at S09 E72. The solar wind measured at the *ISEE 3* spacecraft was $430 \, \mathrm{km \, s^{-1}}$. The neutron-decay particles had access to the observer's magnetic field line at heliocentric distances >0.7 AU, according to the flare heliolongitude and the measured solar wind speed. The percentage of ~ 30 MeV solar neutrons reaching the shadow radius was 22% (78% of the neutrons decayed inside 0.7 AU and never reached the observer's field line). The in situ proton event showed a precursor to the main 25–45 MeV proton event. The peak of the precursor was about one order of magnitude above the background (see Figure 3 in Evenson et al. 1983). Different configurations of the inner solar system at the time of the flare (solar wind speed and flare location) as well as the intensity of the flare can account for differences in the time–intensity profiles of neutron-decay particles observed at 1 AU (Ruffolo 1991). Moreover, these parameters fix the minimum neutron energy contributing to the particle flux detected at 1 AU (Dröge et al. 1996).

2.2. Simulations

We have developed a model that allows us to get an estimation of the proton intensities at the spacecraft location resulting from the in-flight decay of solar flare neutrons. We consider the impulsive release of a large number of solar neutrons at the Sun. We use the neutron production code developed by Hua et al. (2002) and based on the loop model by Hua et al. (1989) to calculate the neutron spectrum escaping the Sun during a large γ-ray flare (see also Murphy et al. 2007). The code provides the neutron spectrum escaping the Sun at different angles from the flare zenith, normalized to one accelerated proton above 30 MeV.

We assign to each neutron a direction of propagation, α_1, based on the neutron energy-integrated angular-dependent spectrum, that covers the half of the heliosphere outside the neutron shadow (see Figure 1). The energy of each neutron follows the energy distribution for the chosen direction.

Each neutron is assigned a decay time following the exponential distribution in Equation (1). We calculate the radial distance that each neutron is able to travel before it decays, r_1 (see Figure 1). Once the solar neutron decays, we simulate the subsequent proton transport along an IMF line. The decay protons initially travel in the same direction as the parent neutron or radially away from the Sun with pitch-angle ψ (see Figure 1).

For simplicity, we assume scatter-free propagation along the IMF. By taking into account the conservation of the first adiabatic invariant, we calculate the time the daughter proton needs to reach 1 AU and the pitch-angle cosine, μ, when it reaches the observer. We also calculate the heliolongitude at which it is observed, α_2 (see Figure 1). All these quantities can be analytically calculated for a Parker spiral magnetic field.

The results can be expressed in terms of near-Earth differential intensities. We use a three-dimensional array with dimensions of time, energy, and pitch angle to register the neutron-decay protons arriving at 1 AU in a given $\Delta\alpha$ interval. The differential intensities, i.e., the number of particles per unit time, unit energy, unit solid angle, and unit area are given by

$$I = \frac{\hat{N}_\mu}{\Delta t \, \Delta E \, 2\pi \Delta\mu \, A}, \qquad (2)$$
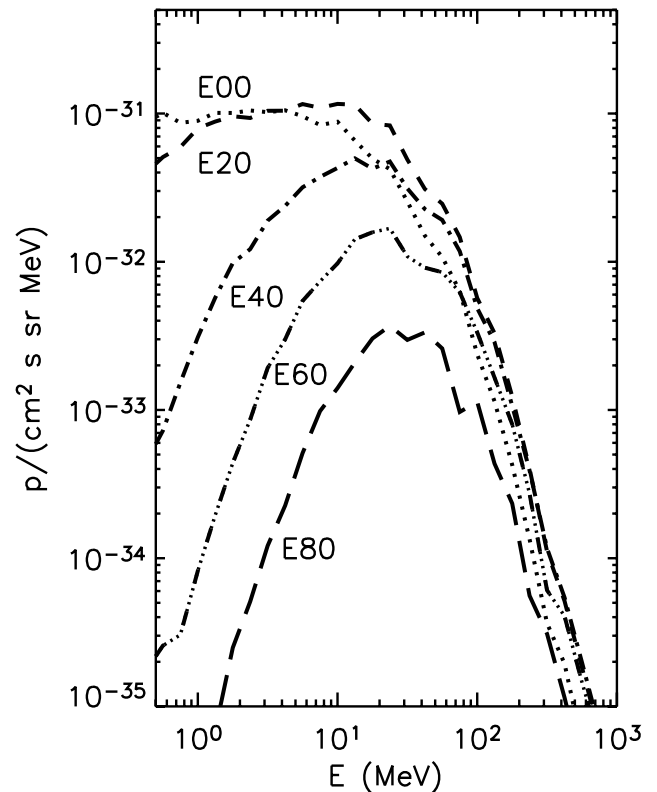

Figure 3. Neutron-decay proton spectrum near the Earth normalized to one accelerated proton above 30 MeV for flare heliolongitudes between E00° and E80° assuming a solar wind speed of $400 \, \mathrm{km \, s^{-1}}$.

where $\hat{N}_\mu$ is the E–μ–t matrix of the registered particles per total number of simulated particles; the subscript μ indicates that each particle has been weighted by $1/\mu$ when registered in the matrix; and $\Delta t, \Delta E$, and $\Delta\mu$ correspond to the bin sizes of the registration matrix. The collecting area is given by $A = r_\oplus^2 \Delta\alpha \cos \psi_\oplus$, where $r_\oplus$ equals 1 AU, $\cos \psi_\oplus = (\sqrt{1 + (r_\oplus \Omega/u)^2})^{-1}$, u is the solar wind speed, and Ω is the sidereal solar rotation rate.

Figure 3 shows the neutron-decay proton spectrum near the Earth normalized to one accelerated proton above 30 MeV for flare heliolongitudes between E00° and E80°. We assumed a solar wind speed of $400 \, \mathrm{km \, s^{-1}}$. It can be seen that the smaller the heliolongitude of the parent flare, the larger the intensities at 1 AU. Note that for a small shadow radius the observer's magnetic flux tube captures a big fraction of the neutron-decay protons. On the other hand, most of the solar neutrons decay before being able to reach the observer's magnetic field line if the solar flare is located at E80°; then the shadow radius is about 0.9 AU. The spectrum shown in Figure 3 would need to be scaled for different flare sizes (i.e., number of protons above 30 MeV that interacted with the atmosphere) to be compared with observations.

3. DATA ANALYSIS

We analyze in situ proton and electron intensities observed by the semi-conductor detector telescopes (SST) detector of *Wind*/3DP (Lin et al. 1995), which provides measurements of the differential intensities of 1–11 MeV protons and 0.025–1 MeV electrons. The *Wind* spacecraft was launched in 1994, and during the first three years of the mission the spacecraft was placed in a highly elliptical orbit (with apogee $\sim 60 R_\oplus$) around the Earth. In 1997 October, a lunar flyby sent the spacecraft into an eight

Table 1
East X-class Solar Flare Candidates in Solar Cycle 23

	Solar Flare				Solar Wind		Neutron Horizon		
Date (1)	Start[a] (UT) (2)	Rise[a] (minutes) (3)	X-ray Class (4)	Hα Position (5)	Speed (km s^{-1}) (6)	Footpoint (°) (7)	d_{min} (AU) (8)	E_{min}^n (MeV) (9)	Percent at 10 MeV (%) (10)
2001 Jun 23	04:02	6	X1.2	E23N10	487 ± 30	49	0.01	0.03	96
2001 Sep 24	09:32	66	X2.6	E23S16	455 ± 5	53	0.02	0.04	93
2004 Jul 16	01:43	23	X1.3	E41S11	434 ± 5	55	0.16	3.63	55
2004 Jul 16	10:32	9	X1.1	E36S10	419 ± 8	57	0.12	1.88	64
2004 Jul 16	13:49	6	X3.6	E35S11	404 ± 5	60	0.13	2.25	61
2004 Jul 17	07:51	6	X1.0	E24S11	553 ± 16	43	0.01	0.01	96
2005 Jan 1	00:01	30	X1.7	E34N06	447 ± 9	54	0.06	0.50	80
2005 Jan 15	00:22	21	X1.2	E08N14	635 ± 11	38	0.00	0.00	100

Note. [a] The start time is the time at which the flare emission officially begins in soft X-rays (1–8 Å). The rise time is the time interval between the start time and the peak time of soft X-ray flux.

month halo orbit around the L1 point, where it remains since 2004 May (see Wang 2009 for more details).

In this section, we first select the most intense flares occurring in the eastern hemisphere of the Sun in solar cycle 23. Then we characterize the IMF after the occurrence of each flare and we finally check if a particle event could occur in isolation. The goal is to identify the best time periods for the observation of protons and electrons from the in-flight decay of solar neutrons.

3.1. Heliospheric Configuration

We use the *SolarSoft*[6] catalog to access the timing, class, and location of all solar flares observed during solar cycle 23, from 1996 May 1 to 2007 December 31. We find 22,847 flares, of which 126 are GOES X-class flares. Forty-four X-class flares have no location assigned. We use Solar Geophysical Data,[7] Solar Monitor,[8] and the Space Weather Reports[9] to identify these locations, resulting in a sample with a total of 53 X-class flares located in the solar eastern hemisphere.

For each solar flare in this sample, we calculate the distance at which the neutron horizon intersects with the Parker spiral, i.e., the shadow radius. As we saw in the previous section, this distance depends on the flare location and on the solar wind speed. We use the solar wind data provided by *Wind*/3DP to estimate the average solar wind speed, taking a 2 hr interval after the start time of the flare emission.

Finally, we calculate the energy of the neutrons that can reach the shadow radius in the neutron mean lifetime, obtaining the minimum neutron energy, E_{min}, that may contribute to the particle flux detected at 1 AU. We find 27 eastern hemisphere flares for which the neutron-decay protons could be detected by *Wind*, that is, with $E_{min} < 11$ MeV.

3.2. Solar Energetic Particle Intensities

We examine the in situ 50–394 keV electron and 1–11 MeV proton intensities measured by *Wind* following each flare. We exclude seven flares from the sample because the energetic electron events at 1 AU show spikes associated with Earth's bow shock, and the 1–11 MeV proton intensities remain stable but at high levels (for these events the spacecraft was located at less than $65 R_\oplus$ from the Earth).

Twelve of the remaining 20 solar flares occurred during periods of enhanced proton intensities in the interplanetary medium, due to previous SEP events (in some cases associated with flares in the western hemisphere of the Sun and coronal mass ejections that were accompanied by interplanetary shocks crossing 1 AU). Table 1 lists the eight eastern hemisphere flares in the final sample. Columns 1–5 give the details of each solar flare (timing, class, and location). Columns 6 and 7 give the mean value of the solar wind speed and the heliolongitude of the corresponding nominal footpoint of the IMF line connecting the observer to the Sun. Columns 8–10 list the distance along the neutron horizon to the observer's IMF line, the minimum neutron energy contributing to the particle flux detected at 1 AU, and the percentage of solar neutrons remaining at 10 MeV when they reach the shadow radius.

We find two flares in 2001, four flares in 2004, and two flares in 2005, with heliolongitudes ranging from E00° to E40°. Most of them are X-ray solar flares between X1 and X2; the largest flare is an X3.6. In all cases, any previous west flare was observed more than 1 day before the occurrence of the east flare candidate, and any subsequent flare observed in the west hemisphere of the Sun occurred at least 3 hr later.

The mean solar wind speed derived for each event ranged from 400 to 650 km s^{-1}, with a mean standard deviation below 30 km s^{-1}. The values of d_{min} vary between 0 and 0.16 AU, being zero for the central meridian flare that occurred on 2005 January 15. In four cases, the neutron horizon intersects the observer's magnetic field line very close to the Sun ($d_{min} < 0.02$ AU), while for the other cases, 0.05 AU $< d_{min} < 0.16$ AU. The minimum neutron energy that may contribute to the particle event observed at 1 AU is smaller than 4 MeV.

4. RESULTS

Figure 4 shows the calculated percentage of remaining 10 MeV neutrons at the shadow radius, as a function of east flare heliolongitude and solar wind speed. The blue dots show the values for the eight events in the sample. In four cases more than 90% of the 10 MeV neutrons have not yet decayed when they reach the observer's magnetic field line, due to the fact that d_{min} is small (<0.02 AU).

Figure 5 shows the 50–394 keV electron and 1–11 MeV proton intensities observed by *Wind*/3DP following these four flares. Only for the largest (X2.6) solar flare (2001 September 24), the in situ electron and proton intensities rise above
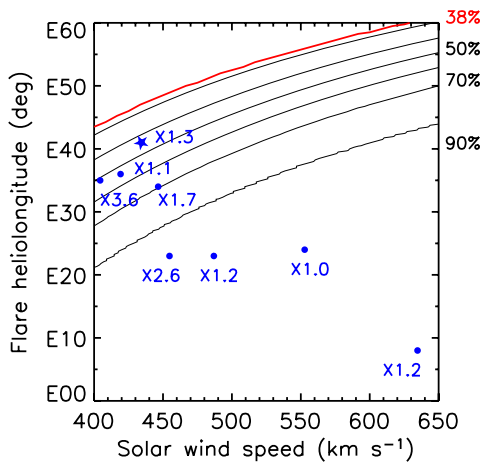
Figure 4. Percentage of remaining neutrons that reach the shadow radius at 10 MeV, as a function of the flare heliolongitude and the solar wind speed. Blue dots show the solar wind speeds and flare heliolongitudes for the eight flares in Table 1. The 2.223 MeV neutron-capture γ-ray line emission was observed for the 2004 July 16 flare (denoted by a star).

(A color version of this figure is available in the online journal.)

background in the $\sim$7 hr time interval following each solar flare. Note however that since $d_{\min}$ is small and a fast halo CME was associated with this event, it is impossible to distinguish the primary solar energetic protons from the neutron-decay ones using in situ observations at 1 AU. The electron intensity profiles show a small precursor coincident with the timing of the solar hard X-ray emission observed by the Hard X-Ray Spectrometer (Fárník et al. 2001). Thus, it is plausible that the precursor is due to hard X-ray contamination. No precursor is observed in the 1–11 MeV proton intensity profiles. For most of the events, the background intensities remain around 10^{-7} protons (cm^2 sr s eV)$^{-1}$ in the 3–6 MeV energy channel.

Figure 6 shows the in situ electron and proton intensities observed after the other four flares in the sample, with values of $d_{\min}$ between 0.06 AU and 0.16 AU (remaining neutron percentages ranging from 80% to 55%). No proton event is observed in the 7 hr period following these solar flares.

For completeness, we analyzed the proton intensities measured at higher energies (6–60 MeV) by the Energetic and Relativistic Nucleon and Electron Experiment (ERNE) on board the *Solar and Heliospheric Observatory* (*SOHO*; Torsti et al. 1995), during the dates listed in Table 1. *SOHO*/ERNE did not observe any particle intensity increase above background on these dates. This suggests that solar neutrons, if present during these events, produced neutron-decay proton events that remained below the background intensities.

Shih et al. (2009) analyzed *RHESSI* measurements (Lin et al. 2002) from 2002 to 2005 of the 2.223 MeV neutron-capture γ-ray line emission of 29 solar flares. For the flares in Table 1, the 2.223 MeV neutron-capture γ-ray line was only observed for the 2004 July 16/01:43 UT solar flare, at the *RHESSI* detection limit. Since no event was observed by either *Wind* or by *SOHO* on this date, we assume that the low-energy neutron-decay proton event remained below the background intensities.

5. DISCUSSION

Figure 7 shows the background spectrum of the 1–11 MeV proton intensities measured by *Wind*/3DP and *SOHO*/ERNE on 2004 July 16. Intensities measured by *Wind* in the 6–11 MeV energy range are a factor of four above the intensities measured by *SOHO*.

Based on the measured fluence of the 2.223 MeV neutron-capture γ-ray line observed by *RHESSI* on 2004 July 16/01:43 UT, Shih et al. (2009) estimated that 7.7×10^{28} protons >30 MeV interacted with the solar atmosphere, assuming an accelerated ion spectral index of 3.75. For this flare size, we calculate the neutron-decay proton spectrum near the Earth. The solid curve in Figure 7 shows the expected neutron-decay proton spectrum assuming 7.7×10^{28} protons above 30 MeV, a spectral index of 3.5 at the Sun and the heliospheric configuration of that day (solar wind speed of $\sim$400 km s^{-1}, flare located at E40). It can be seen that the neutron-decay proton spectrum expected for the GOES X3.4 flare of 2004 July 16 is well below the observed background spectrum.

The largest fluence of the 2.223 MeV neutron-capture γ-ray line reported by Shih et al. (2009) was observed on 2003 October 28 associated with an X17 solar flare when >9.5×10^{32} protons above 30 MeV interacted with the solar atmosphere. We calculate the number of neutrons escaping the Sun and estimate the neutron-decay proton spectrum near the Earth for different flare locations. It can be seen that for a giant event like 2003 October 28, the neutron-decay proton event would be well above the *Wind*/3DP background for heliolongitudes of up to E60°. This indicates that *Wind* is in principle able to detect neutron-decay protons, but only if a giant event is detected in isolation of any other enhancements (earlier events or primary particles from the same flare event).

6. CONCLUSIONS

We presented a search for evidence of in situ electrons and protons resulting from the decay of low-energy (<10 MeV) solar flare neutrons. We selected a sample of isolated X-class eastern hemisphere flares through solar cycle 23 occurring during quiescent conditions in the interplanetary medium. We found no evidence in the in situ data of the decay products of solar flare neutrons in the sample.

Solar γ-ray emission was observed at the *RHESSI* detection limit for one of the flares in the sample. We used theoretical calculations of the neutron spectrum escaping the Sun, combined with an interplanetary propagation model to estimate the near-Earth neutron-decay proton spectrum. We found that the simulated neutron-decay proton spectrum is well below the observed background proton spectrum. Assuming the largest number of protons above 30 MeV reported by Shih et al. (2009) and the best case configuration for the observation of low-energy neutron-decay protons by *Wind*, we found that the spectrum would be above the background for flare heliolongitudes up to E60°.

Future missions, such as *Solar Probe+* and *Solar Orbiter*, will provide measurements made in the inner heliosphere at radial distances <1 AU. Such measurements have the potential of detecting decay products of low-energy (1–10 MeV) neutrons, due to the fact that their intensities are higher in the inner heliosphere; $\sim$65% of the 10 MeV neutrons decay before reaching 0.3 AU.
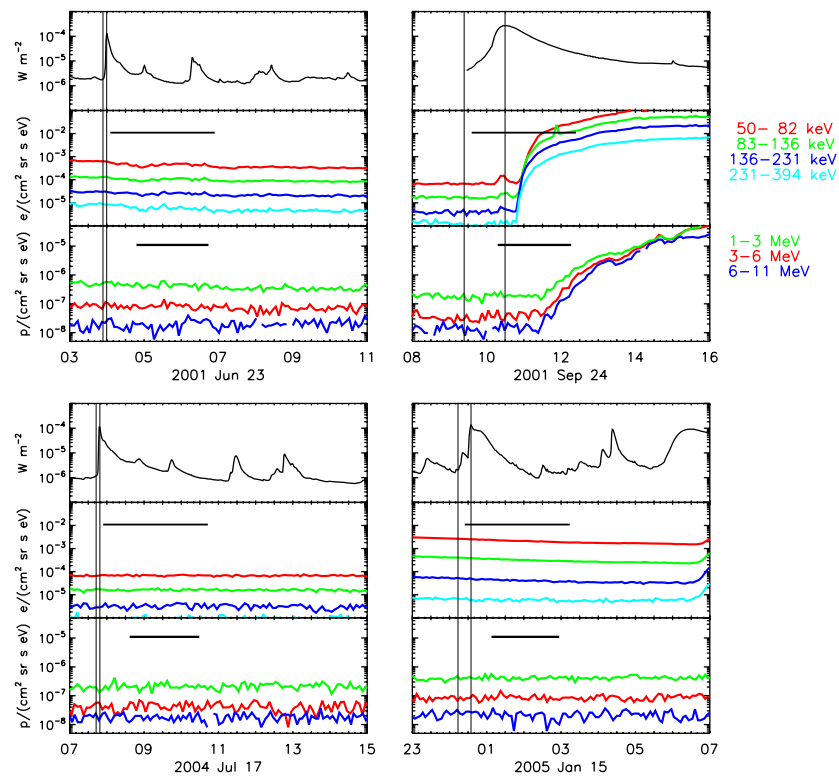
Figure 5. From top to bottom: soft X-ray flux observed by *GOES* and electron (50–394 keV) and proton (1–11 MeV) intensities measured in situ by *Wind*/3DP for time periods associated with the four solar flares in Table 1. The thin vertical lines show the onset time and the peak time of the soft X-ray flux. The gray rectangles show the expected arrival time intervals of the 50–394 keV electrons and 1–11 MeV protons that arise from the in-flight decay of solar neutrons and propagate scatter-free along the IMF.

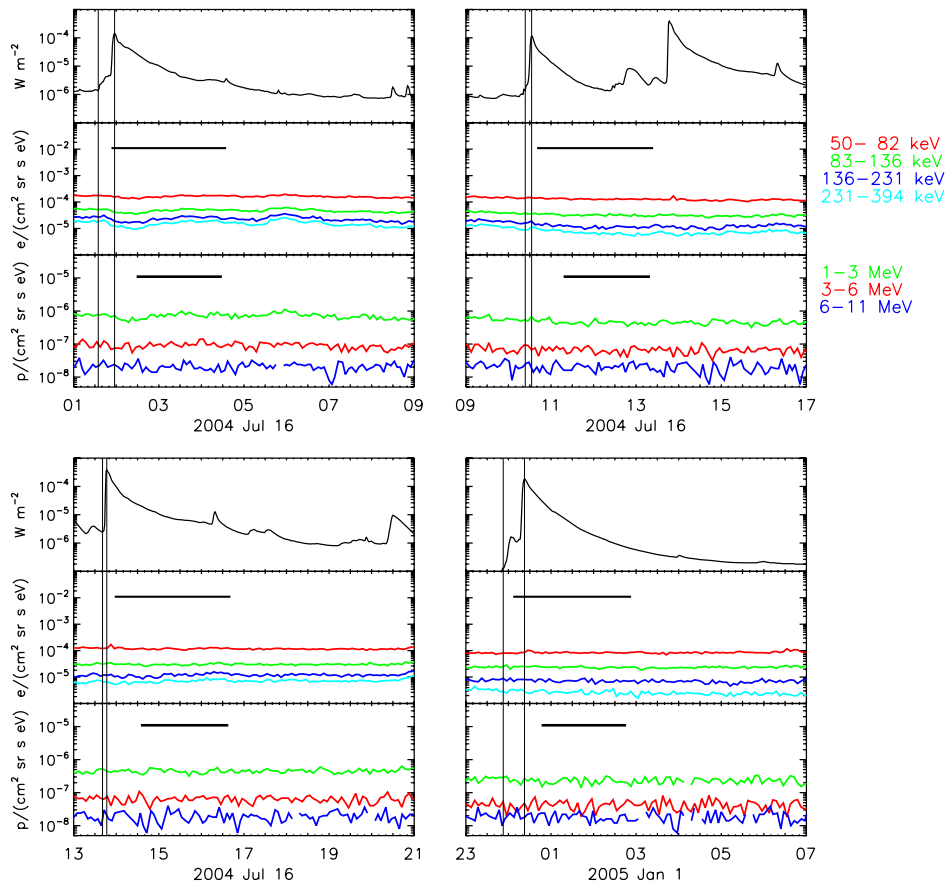(A color version of this figure is available in the online journal.)

Figure 6. Same as in Figure 5 but for the remaining four solar flares in Table 1.

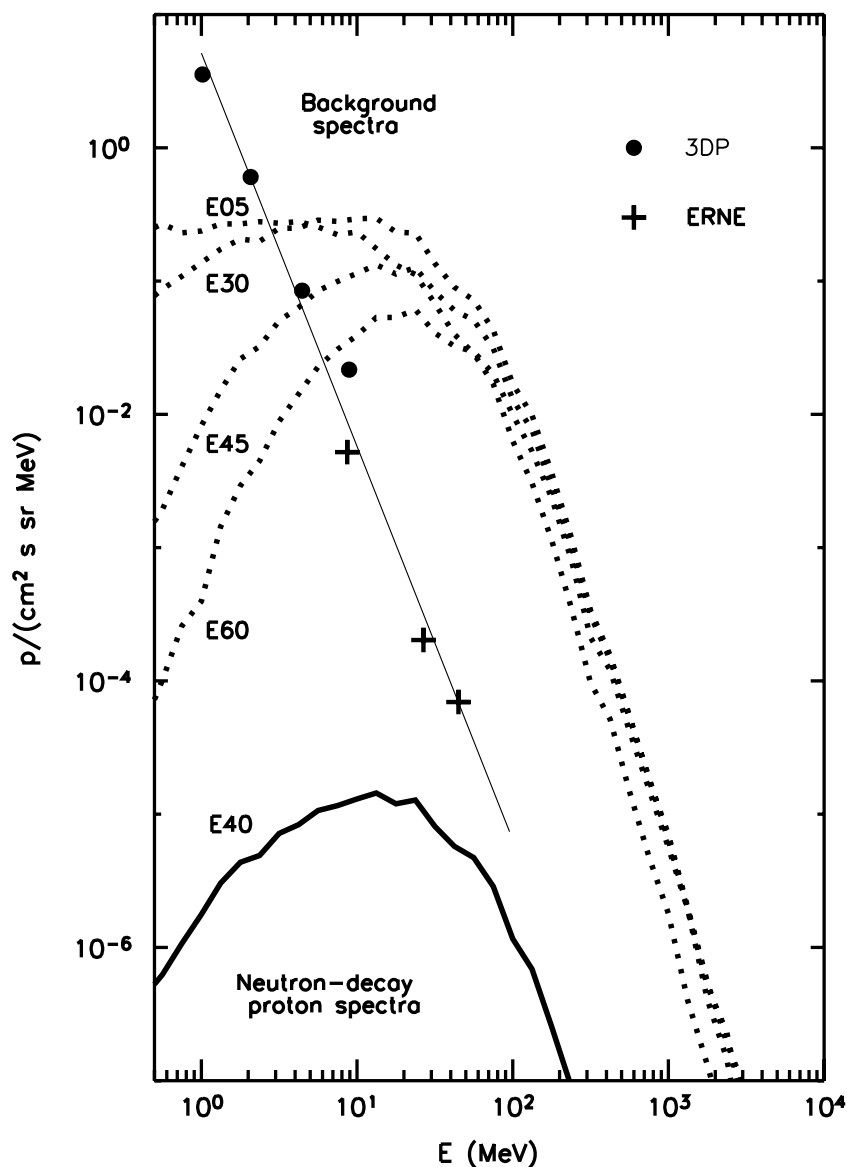(A color version of this figure is available in the online journal.)

6

Figure 7. Background proton spectrum observed on 2004 July 16 (solid line). Simulated neutron-decay proton spectrum near the Earth (solid curve) assuming that 7.7×10^{28} protons above 30 MeV interacted with the solar atmosphere. The dotted curves show the expected spectrum assuming 9.5×10^{32} protons >30 MeV (value for the 2003 October 28 flare) for three different flare heliolongitudes. Hence, if occurring in isolation, the event should be detectable by *Wind*/3DP above ∼5 MeV for flare heliolongitudes smaller than E60°.

REFERENCES

Chupp, E. L., et al. 1987, ApJ, 318, 913
Daibog, E. I., & Stolpovskii, V. G. 1987, Sov. Astron. Lett., 13, 458
Dröge, W., Ruffolo, D., & Klecker, B. 1996, ApJ, 464, L87
Evenson, P., Kroeger, R., Meyer, P., & Reames, D. 1990, ApJS, 73, 273
Evenson, P. A., Kroeger, R., & Meyer, P. 1985, Proc. ICRC (Goddard Space Flight Center), 130
Evenson, P., Meyer, P., & Pyle, K. R. 1983, ApJ, 274, 875
Fárník, F., Garcia, H., & Karlický, M. 2001, Sol. Phys., 201, 357
Feldman, W. C., et al. 2010, J. Geophys. Res., 115, 1102
Hua, X., Kozlovsky, B., Lingenfelter, R. E., Ramaty, R., & Stupp, A. 2002, ApJS, 140, 563
Hua, X., & Lingenfelter, R. E. 1987, Sol. Phys., 113, 229
Hua, X., Ramaty, R., & Lingenfelter, R. E. 1989, ApJ, 341, 516

Kocharov, L. G., Torsti, J., Vainio, R., Kovaltsov, G. A., & Usoskin, I. G. 1996, Sol. Phys., 169, 181
Lin, R. P., et al. 1995, Space Sci. Rev., 71, 125
Lin, R. P., et al. 2002, Sol. Phys., 210, 3
Lingenfelter, R. E., & Ramaty, R. 1967, in High Energy Nuclear Reactions in Solar Flares, ed. B. S. P. Shen (New York: Benjamin), 99
Murphy, R. J., Kozlovsky, B., Share, G. H., Hua, X., & Lingenfelter, R. E. 2007, ApJS, 168, 167
Parker, E. N. 1958, ApJ, 128, 664
Ramaty, R., & Murphy, R. J. 1987, Space Sci. Rev., 45, 213
Roelof, E. C. 1966, J. Geophys. Res., 71, 1305
Ruffolo, D. 1991, ApJ, 382, 688
Ryan, J., et al. 1993, Proc. ICRC (Alberta), 103
Share, G. H., Murphy, R. J., Tylka, A. J., Kozlovsky, B., Ryan, J. M., & Gwon, C. 2011, J. Geophys. Res., 116, A03102
Shea, M. A., Smart, D. F., & Pyle, K. R. 1991, Geophys. Res. Lett., 18, 1655
Shih, A. Y., Lin, R. P., & Smith, D. M. 2009, ApJ, 698, L152
Torsti, J., et al. 1995, Sol. Phys., 162, 505
Wang, L. 2009, PhD thesis, Univ. California, Berkeley